TUTORIAL REVIEW

Check for updates

Ionic liquids as a new cornerstone to support hydrogen energy

Yanrong Liu,[a,b,c] Jiayao Cui,[a,d] Hao Wang, ID [a,b,c] Ke Wang, ID [a,b,c] Yuan Tian,[a,e] Xiaoyi Xue,[b] Yueyang Qiao,[b] Xiaoyan Ji[f] and Suojiang Zhang ID *[a,b,d]

As a fuel or energy carrier, hydrogen has been identified as a key way to decarbonize electricity, industry, transportation, and heating sectors. Hydrogen can be produced by a variety of methods, among which water electrolysis driven by renewable energy is sustainable and nearly carbon-free. To use hydrogen widely, storage and transportation over long distances are another key issue. Apart from storage at high pressure and low temperature, hydrogen can be stored in organic compounds *via* chemical bonding under relatively mild conditions. Efficient utilization of hydrogen includes hydrogen fuel cells as an alternative to internal combustion engines. From the above scenarios, catalysis and reaction media are the key factors for realizing hydrogen energy implementation. Ionic liquids (ILs) offer new opportunities due to their tunable functional groups, low vapor pressure, and stable structures as additives, solvents, and charge transfer materials. ILs are known to produce solid catalysts with controllable properties, decorate solid catalysts with modified electrons and geometric structures, and serve as electrolytes and hydrogen storage media. This review summarizes and recaps the recent progress in how ILs act as a cornerstone to support the production, storage, and utilization of hydrogen. Furthermore, critical challenges and future research directions of ILs in hydrogen energy applications are also outlined.

Introduction

As the world's population is growing and living standards are improving, the demand for energy is significantly growing. By far, the vast majority of the world's energy demand is still dependent on fossil sources (*e.g.*, petroleum, natural gas, and coal), leading to energy crises, carbon dioxide (CO_2) emissions, and even political tensions. Therefore, it is urgent and necessary to find new and clean energy sources that can reduce carbon emissions to accelerate the energy transition, especially in industry and transportation sectors.[1] Hydrogen is the most abundant element on Earth and has been explored as a prom-

ising energy carrier due to its high energy density as well as its renewable and green nature.[2–4] In particular, surplus power from renewable energy can be converted into hydrogen and stored as a back-up. During the peak load periods on the grid, power generated by hydrogen can be fed into the grid. Such a way significantly improves the utilization efficiency of renewable energy, reduces abandoned wind and solar energy, enhances grid dispatchability, and ensures grid security. Therefore, hydrogen energy is critical to the future construction of a multi-energy supply system, which may represent a longstanding clean energy solution. By 2050, hydrogen energy is expected to support 18% of global energy,[5] and countries are taking ambitious action to seize this opportunity toward carbon neutrality.[6,7]

Hydrogen does not purely exist in nature, and its production relies heavily on energy input. It can be manufactured from various sources, including both renewable and non-renewable sources. Hydrogen production from fossil fuels has reached the highest level of technical readiness, but the process is accompanied by large emissions of CO_2. Further purification and carbon capture and storage techniques require additional costs. Hydrogen production through water electrolysis has the advantages of high purity and zero carbon emissions and has been identified as the most promising green hydrogen supply technology for the future.[8] The challenge associated with water electrolysis is high power

*a*Beijing Key Laboratory of Ionic Liquids Clean Process, CAS Key Laboratory of Green Process and Engineering, State Key Laboratory of Multiphase Complex Systems, Institute of Process Engineering, Chinese Academy of Sciences, Beijing 100190, China. E-mail: yrliu@ipe.ac.cn

*b*Longzihu New Energy Laboratory, Zhengzhou Institute of Emerging Industrial Technology, Henan University, Zhengzhou 450000, P. R. China

*c*Huizhou Institute of Green Energy and Advanced Materials, Huizhou, Guangdong 516081, China

*d*School of Chemical Engineering, University of Chinese Academy of Sciences, Beijing 100049, China

*e*Tianjin Key Laboratory of Molecular Optoelectronic Sciences, Department of Chemistry, School of Science, Tianjin University, Tianjin 300072, China

*f*Energy Engineering, Division of Energy Science, Luleå University of Technology, 97187 Luleå, Sweden

consumption, which originates from the low efficiency of the electrodes, requiring active, durable, and inexpensive electrocatalysts as well as low fluid-resistance electrolyzers.[9]

Another obstacle that hinders hydrogen energy implementation is the cost and immaturity of hydrogen storage under mild conditions. The compressed-gas and cryogenic-liquid hydrogen storage not only causes high energy penalties and rigorous requirements for containers but may also raise safety concerns. Hydrogen storage alloys have the advantages of high safety and high hydrogen purity but face problems of low gravimetric capacity and slow kinetics. New hydrogen storage media are desirable, such as liquid organics.[10] In such media, dehydrogenation is a catalytic process using highly efficient catalytic agents.[11] Recently, ammonia has also been realized as a hydrogen storage carrier. Although it requires large amounts of energy for cracking and the subsequent hydrogen compression at the end-user site, ammonia is easily liquefied for transportation.[12] Ammonia produced by the traditional Haber–Bosch method results in giant carbon emissions. The new method through electrocatalysis using N_2 and water to produce ammonia under ambient conditions is promising but requires electrocatalysts to activate inert N_2 and suppress byproduct formation.

The hydrogen fuel cell, in which hydrogen reacts with oxygen to produce electricity, is one of the most iconic technologies for the utilization of hydrogen. Hydrogen fuel cells are promising candidates to replace internal combustion engines without the limitations of the Carnot cycle and have been proven to be desirable for heavy-duty vehicles. The critical challenge is the sluggish kinetics of the oxygen reduction reaction (ORR) at the cathode. The current catalyst of choice is platinum (Pt), but its cost, mass activity, and durability are still unsatisfactory. Recent efforts have concentrated on reducing the Pt loading through alloying with Earth-abundant metals. In addition, new catalytic interfaces are also desirable to improve ion and charge transfer as well as mass transport, and to avoid corrosion.[13]

To ensure that hydrogen energy is more secure and affordable to release its potential, critical issues must be addressed. The abovementioned scenarios for hydrogen production, storage, and application share common problems of high cost, low efficiency, and poor stability of catalysts. Ionic liquids (ILs) could offer a solution to these problems. ILs are capable of facilitating electrocatalysis and thermocatalysis in the following ways: (1) ILs are known to act as surfactants or stabilizers to regulate the shape, particle size, and defect level of catalyst particles, thereby enhancing catalyst intrinsic activity and active site density;[14] (2) ILs can be designed to contain metal and metal-free elements, which serve as sacrificial precursors to produce catalysts;[15] (3) ILs can be immobilized on the surface of a solid catalyst to form a solid catalyst with an IL layer (SCILL) and regulate catalytic activity, durability, and selectivity;[16] (4) ILs are favorable electrolytes or electrolyte additives due to their high ionic conductivity;[17] and (5) ILs can serve as hydrogen storage media that can be hydrogenated based on imidazole or phenyl rings[18] or can serve as additives to activate amineborane-based materials.[19] Although ILs have the advantages described above, there are still concerns about their biological and environmental toxicity, which require careful handling during the process.[20]

Therefore, improving the intrinsic activity and active site density by rational design of ILs and IL–particle interactions is a new concept for enhancing the efficiency of electrocatalytic and thermocatalytic processes involved in hydrogen energy. In this respect, ILs will serve as a new cornerstone to support the implementation of hydrogen energy. ILs have been proven to be excellent electrolytes and catalysts and assist in materials synthesis.[21–25] While some insightful reviews have summarized IL applications in several scenarios, such as the hydrogen evolution reaction (HER),[15,26] hydrogen storage[27] and fuel cells,[28] the overall picture of how ILs support hydrogen energy is still missing. This review provides a summary of the recent progress in IL assistance in producing solid catalysts and IL–catalyst interactions, and their success in facilitating hydrogen

Yanrong Liu is an Associate Professor at the Institute of Process Engineering (IPE), Chinese Academy of Sciences (CAS). She received her PhD in Chemical Engineering from the Technical University of Denmark in 2018. She worked as a postdoc at the Division of Energy Science/Energy Engineering at the Luleå University of Technology, Sweden. Her research interests mainly focus on the design and application of ionic liquids, hydrogen energy technologies, and electrochemical small molecule conversion.

Yanrong Liu

Prof. Suojiang Zhang is a Professor and Director General of the Institute of Process Engineering (IPE), Chinese Academy of Sciences (CAS), an academician of CAS and a Fellow of the RSC. He received his PhD in Physical Chemistry from Zhejiang University in 1994. He currently serves as the Editor-in-Chief of Green Energy & Environment *(GEE),* Green Chemical Engineering *(GreenChE) and* Process Engineering Journal of China*. His research focuses on ionic liquids, green process engineering, and large-scale energy storage.*

Suojiang Zhang
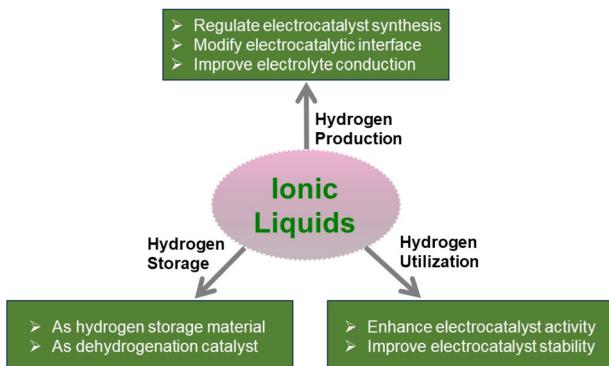
Scheme 1 The application of ionic liquids in hydrogen energy.

production, storage, and application (Scheme 1). As we have recently carried out comprehensive reviews of the use of ILs in synthetic ammonia,[29,30] this part will not be included in this review. Finally, critical challenges and perspectives on future research on IL applications in hydrogen energy are also highlighted.

Application of ionic liquids in water electrolysis

The advantages of ILs in facilitating water electrolysis are mainly reflected in the synthesis of highly efficient electrocatalysts where the particle size, active site exposure, and electronic structures can be controlled by the interfacial microenvironment. Additionally, ILs can act as binders and electrolytes to accelerate ion transfer and mass transport during water electrolysis. The research work from these aspects is reviewed in this section.

Ionic liquids to regulate electrocatalyst synthesis

Due to steric hindrance, static electricity, viscosity stability, and solvation forces, ILs have been used in the synthesis of electrocatalysts to control their structure, morphology, and properties, and such successes have also been applied to water electrolysis, *i.e.*, in the preparation of highly active and durable electrocatalysts for the cathodic HER and the anodic oxygen evolution reaction (OER). The HER performance of the ILs controlled electrocatalyst is summarized in Table 1.

Lau *et al.* investigated the effects of aromatic and non-aromatic ILs on the synthesis of MoS_2 as an HER electrocatalyst. It was found that the MoS_2 regulated by [BMIM][TfO] and *N*-butylpyridinium trifluoromethanesulfonate ([BPy][TfO]) had higher crystallinity and possessed more unstacking/de-layering structures compared to those regulated by non-aromatic ILs,[31] and such a high edge exposure was desirable for HER occurrence. The MoS_2 synthesized in [BMIM][TfO] had the best HER performance, delivering 529 μA at −533 mV, which benefited from the effects of strong molecular interactions, H-bond

acidity, and aromatic properties of ILs on the structure of MoS_2. Liu *et al.* presented the mediation of [BMIM][BF$_4$] to prepare MoS_2/NG composites.[32] Through electrostatic interactions, [BMIM][BF$_4$] stabilized the edge sites of MoS_2 and induced a delaminating morphology of the MoS_2 crystals, thereby enhancing the HER electrocatalytic activity. In particular, with the addition of 1.0 mL [BMIM][BF$_4$], the acquired MoS_2/NG-IL10 displayed high HER performance and achieved 136.3 mA cm^{-2} at an overpotential of 300 mV in 0.5 M H$_2$SO$_4$, which is 7.4 times greater than that of MoS_2 without [BMIM][BF$_4$] mediation. Zhang *et al.* used [BPy][Br] as a structure directing agent to synthesize 1T/2H-MoS_2.[33] The result indicated that the proportion of the metal 1T phase in 1T/2H-MoS_2 can be increased due to steric hindrance and the π-stacking interaction of [BPy][Br], thus promoting active site exposure and enhancing charge transfer. When the proportion of the 1T phase in 1T/2H-MoS_2 reached 91.9%, the best HER performance was achieved with a Tafel slope of 59 mV dec^{-1}. A facile synthesis strategy to directly grow a network of $Co_{0.6}Ni_{0.4}Se_2$-LN on carbon cloth was investigated,[34] where [C$_{12}$MIM][Ac] played an important role in the construction of the 3D hierarchical architecture. The resulting $Co_{0.6}Ni_{0.4}Se_2$-LN has the characteristic of a layered structure with sufficient active sites and channels for the transfer of electrolyte ions and electrons, leading to a low HER overpotential of 163 mV@10 mA cm^{-2} in 0.5 M H$_2$SO$_4$.

ILs can also serve as sacrificial precursors, such as metal sources, carbon sources, and heteroatom sources, to produce electrocatalysts through pyrolysis. To use ILs as metal sources, Zhang *et al.* prepared ordered mesoporous catalysts of MoC@C using [BMIM]$_2$[MoO$_4$].[35] Uniform particle sizes (5 nm) of MoC with a highly crystalline structure were obtained due to the action of SBA-15 silica hard-template mediated pore channels, contributing to a low HER overpotential of 110 mV@10 mA cm^{-2} in 0.5 M H$_2$SO$_4$. Nanostructured Ni$_2$P and Ni$_{12}$P$_5$ were developed using [P$_{4444}$][Cl] as the reaction source by a microwave heating method,[36] which dramatically reduced the reaction time. In 0.5 M H$_2$SO$_4$, Ni$_2$P has a better HER overpotential of 102 mV than Ni$_{12}$P$_5$ of 182 mV at 10 mA cm^{-2}. [P$_{6,6,6,14}$]$_2$[CoCl$_4$] could serve as a source of Co and P for the preparation of Co$_2$P/CNTs by means of a phosphidation step mixed with CNTs,[37] and the resulting Co$_2$P was uniformly distributed on CNTs to acquire only 150 mV at 10 mA cm^{-2} for the HER. Ying *et al.* used [OA][H$_2$PO$_2$] as a source of P to produce Ni$_2$P$_4$O$_{12}$.[38] The [OA][H$_2$PO$_2$] assisted synthesis not only speeds up the reaction process, but also offers a rich source of P for the manufacturing of metaphosphate, resulting in a low HER overpotential of 116 mV at 10 mA cm^{-2} in 1.0 M KOH. [BMIM][Cl] was applied as a source of both carbon and nitrogen to prepare NHCS-W.[39] The dielectric constant of the solvent (*e.g.*, water and ethanol) affects the dissociation/association of the IL precursor, thus affecting the morphologies and structures of the prepared carbon spheres. A solvent with a high dielectric constant is beneficial for the formation of hollow structures to enhance the water-splitting performance. The prepared NHCS-W was used as both the cathode and

anode catalysts, which only required 1.61 V to achieve 10 mA cm^{-2}. An eutectic IL of Ni-MA composed of $NiCl_2 \cdot 6H_2O$ and malonic acid with a mole ratio of 1 : 5 was pyrolyzed to produce $NiS_2@GO$.[40] The unique structure of the encapsulated NiS_2 in the GO shell improves the kinetics and the exposure of the active sites. Consequently, the $NiS_2@GO$ electrocatalyst shows both a reduced HER overpotential of 57 mV and an OER overpotential of 294 mV at 10 mA cm^{-2} in 1.0 M KOH. The strategy of using 1-butyl-3-methylimidazolium hexafluoro-phosphate ([BMIM][PF$_6$]) as a dopant to introduce oxygen vacancies in N, P, and F tri-doped $MoS_2/NPF-CoFe_2O_4$ was studied by Sun et al.,[41] showing that [Bmim][PF$_6$] not only modulated the electronic structure of $MoS_2/NPF-CoFe_2O_4$, but also constructed an amorphous structure with abundant oxygen vacancies, contributing to a low OER overpotential of 250 mV at 10 mA cm^{-2} in 0.1 M KOH (Fig. 1).

Poly(ionic liquid)s (PILs) are a special type of IL that have both ionic properties and long chains, and also have the potential in the preparation of water-splitting catalysts. The PIL of PVEIB was applied to prepare an HER catalyst composed of $NiS_2-MoS_2/PVEIB/PPy/GO$.[42] PVEIB played a crucial role in combining NiS_2-MoS_2 and PPy/GO with good stability and induced the formation of the 1T phase in MoS_2, leading to a small HER overpotential of 205 mV@10 mA cm^{-2} in 0.5 M H_2SO_4. Different morphologies of bismuth sulfides (Bi_2S_3) were synthesized by Gao et al. using poly(1-methyl-3-(4-vinyl-benzyl)-imidazolium chloride) (PIL-1), poly(diallyldimethyl-ammonium bis(trifuoromethanesulfonyl)imide) (PIL-2), and poly(3-ethyl-1-vinylimidazolium bromide) (PIL-3) as addi-tives.[43] Notably, owing to the different properties of cations and anions, the backbone architectures of the PILs could be selectively coupled to specific crystal faces, modulated and even templated for sequential growth, thus significantly enhancing their effectiveness in regulating the nucleation and growth of inorganic materials (Fig. 2a–c). As shown in Fig. 2a, nanowires, hexagonal plates, and mesostructured plates of Bi_2S_3 were obtained by adjusting PIL-1, PIL-2, and PIL3,
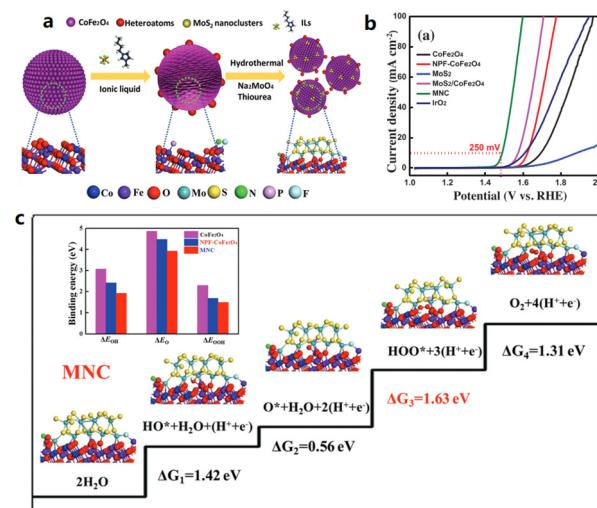
Fig. 1 (a) Schematic illustration of the synthetic strategy for the MNC hybrid, and (b) OER polarization curves without iR-compensation. (c) The elementary steps and binding energies of the intermediates during the OER. Reproduced with permission.[41] Copyright 2018, Wiley-VCH.

respectively. The obtained Bi_2S_3-nanowires showed the best OER performance, close to that of RuO_2 at 10 mA cm^{-2} in 0.1 M KOH. Ding et al. used an IL as the precursor and $CoCO_3$ to form a novel IL containing Co species (Fig. 2d and e),[44] The prepared novel IL was further reacted with CNTs by polymeriz-ation to form a PIL-Co/CNT electrocatalyst with PIL and Co species well dispersed on the CNT surfaces. CoSSPIL/CNT afforded much better OER activity (1.64 V vs. RHE at 10 mA cm^{-2}) compared to Co_3O_4/CNT and $CoCO_3$.

Ionic liquids to modify electrocatalytic interfaces

The electrochemical activity can be improved by modifying the electrode surface and constructing a well-defined solid/liquid or solid/liquid/gas three-phase junction, impacting the charge/ion transfer, mass transport, and hydrophilic/hydro-

Table 1 The HER performance of IL controlled electrocatalysts

ILs	Electrocatalyst	Electrolyte	Overpotential (mV vs. RHE)@10 mA cm^{-2}	Tafel slope (mV dec^{-1})	Entry[ref.]
[BMIM][TfO]	MoS_2	0.5 M H_2SO_4	—	156	1[31]
[BMIM][BF$_4$]	MoS_2/NG	0.5 M H_2SO_4	150	48	2[32]
[BPy][Br]	MoS_2	0.5 M H_2SO_4	259	59	3[33]
[C$_{12}$MIM][Ac]	$Co_{0.6}Ni_{0.4}Se_2$-LN	0.5 M H_2SO_4	163	40	4[34]
[BMIM]$_2$[MoO$_4$]	MoC	0.5 M H_2SO_4	110	—	5[35]
[P$_{4444}$][Cl]	Ni_2P	0.5 M H_2SO_4	102	46	6[36]
[P$_{4444}$][Cl]	$Ni_{12}P_5$	0.5 M H_2SO_4	182	80	7[36]
[P$_{6,6,6,14}$]$_2$[CoCl$_4$]	$Co_2P/CNTs$	0.5 M H_2SO_4	150	47	8[37]
[OA][H$_2$PO$_2$]	$Ni_2P_4O_{12}$	1.0 M KOH	116	97	9[38]
[BMIM][Cl]	NHCS-W	1.0 M KOH	196	101	10[39]
Ni-MA	$NiS_2@GO$	1.0 M KOH	57	47	11[40]
PVEIB	$NiS_2-MoS_2/PVEIB/PPy/GO$	0.5 M H_2SO_4	205	49	12[42]

[BMIM][TfO]: 1-butyl-3-methylimidazolium trifluoromethanesulfonate; [BMIM][BF$_4$]: 1-butyl-3-methylimidazolium tetrafluoroborate; NG: nitro-gen-doped graphene; [BPy][Br]: N-butyl pyridinium bromide; [C$_{12}$MIM][Ac]: 1-dodecyl-3-methylimidazoliumacetate; $Co_{0.6}Ni_{0.4}Se_2$-LN: loofah-like $Co_{0.6}Ni_{0.4}Se_2$; [BMIM]$_2$[MoO$_4$]: 1-butyl-3-methylimidazole molybdate; [P$_{4444}$][Cl]: tetrabutylphosphonium chloride; [P$_{6,6,6,14}$]$_2$[CoCl$_4$]: trihexyl(tetra-decyl)phosphoniumtetrachlorocobaltate; CNTs: carbon nanotubes; [OA][H$_2$PO$_2$]: N-octylammonium hypophosphite; [BMIM][Cl]: 1-butyl-3-methyl-imidazolium chloride; NHCS-W: nitrogen-doped hollow carbon spheres with nanoporous shells; Ni-MA: $NiCl_2 \cdot 6H_2O$: malonic acid 1 : 5; GO: gra-phene oxide; PVEIB: poly(1-vinyl-3-ethylimidazoliumbromide); PPy: polypyrrole
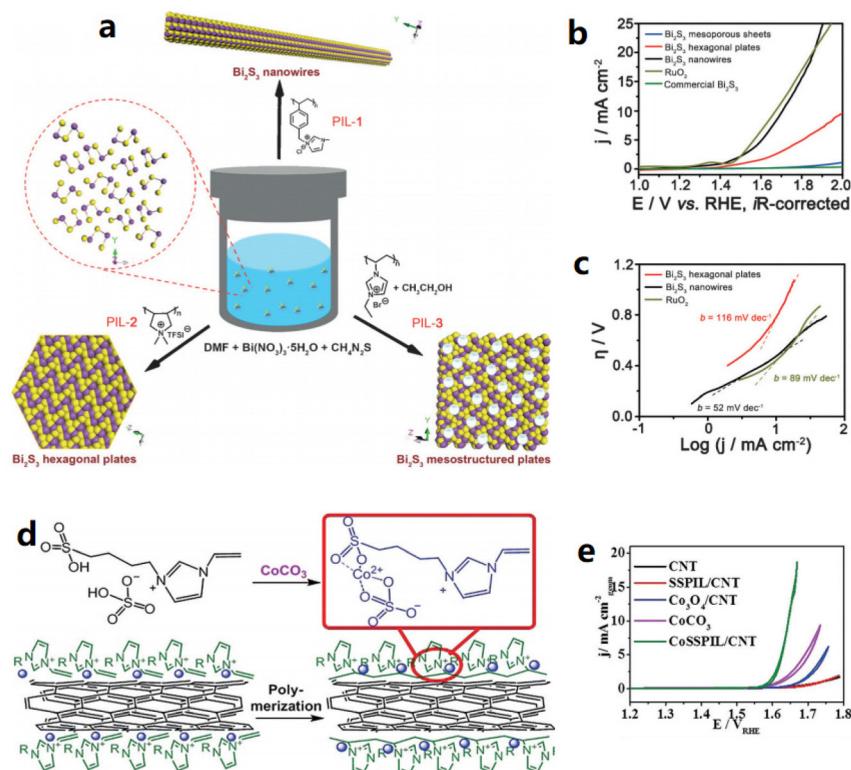
Fig. 2 (a) PILs controlled the structures of Bi_2S_3, (b) OER linear sweep voltammetry (LSV) curves of Bi_2S_3 and RuO_2, (c) Tafel slope of Bi_2S_3 and RuO_2. Reproduced with permission.[43] Copyright 2016, Wiley-VCH; (d) preparation procedure of CoSSPIL/CNT, and (e) cyclic voltammogram (CV) of CoSSPIL/CNT compared to different samples of CNT, SSPIL/CNT, Co_3O_4/CNT, and $CoCO_3$. Reproduced with permission.[44] Copyright 2018, Wiley-VCH.

phobic properties. Gidi *et al.* prepared and characterized hybrid electrocatalysts using *N*-octylpyridinium hexafluorophosphate ([OPy][PF$_6$]) and mineral oil as the binder on multi-walled carbon nanotubes (MWCNTs).[45] The prepared MWCNT/[OPy][PF$_6$] presented high HER electrocatalytic activity and stability in 0.1 M H_3PO_4 solution (pH = 7), as [OPy][PF$_6$] significantly improved the conductive performance and increased the electroactive area of the electrodes. The faradaic efficiency of the MWCNT/OPyPF$_6$ system for hydrogen production was determined to be 60% at −0.30 *vs.* Ag/AgCl, and the sample obtained an extremely high TOF of 16 274. Ji *et al.* used a hydrophobic IL, 1-methyl-2,3,4,6,7,8-hexahydro-1*H*-pyrimidol[1,2-*a*]pyrimidinium bis[(trifluoromethyl)sulfonyl]imide ([MTBD][NTf$_2$]), to modify CoS_2 microspheres where different amounts of IL were used during the evaporation process.[46] All the CoS_2-IL composites exhibited improved OER activity compared to CoS_2 microspheres, and the resulting catalyst could require a low OER overpotential of 310 mV at 10 mA cm^{-2}. The Tafel slope and impedance show improved ionic conductivity and the IL-induced hydrophobic environment at the CoS_2/electrolyte interface provides a favorable microenvironment for triggering the OER process (Fig. 3).

PILs can also be used as surface modifiers. Pham Truong *et al.* demonstrated that the prepared poly(vinyl-imidazolium-
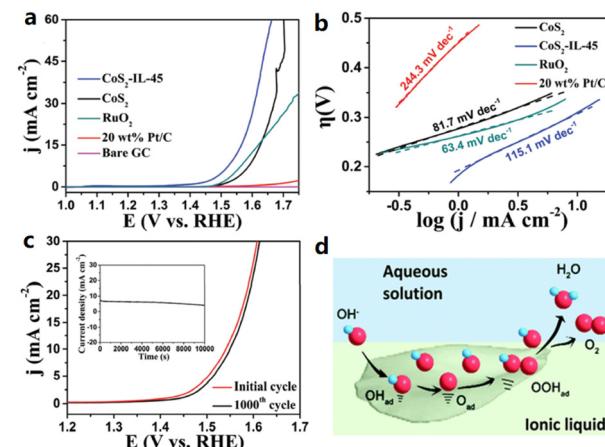
Fig. 3 (a) OER LSV curves of the bare GC electrode, commercial 20 wt% Pt/C, CoS_2 and IL-modified CoS_2 and (b) the derived Tafel plots. (c) OER LSV curves of IL-modified CoS_2 before and after 1000 CV tests. (d) Schematic illustration of the oxidation of water. Reproduced with permission.[46] Copyright 2018, the Royal Society of Chemistry.

methyl), *i.e.*, poly(VImM), enhanced electrocatalytic activity by modifying the Pt catalyst.[47] The hierarchical polymer brush structure accelerated the electron transfer and also the accessibility of water and oxygen. Compared to the Pt/C electrocata-

lyst, Pt/C/poly(VImM) exhibits a higher current density and lower OER overpotential, benefiting from the chemical composition and unique structure of poly(VImM).

Pandey et al. theoretically studied the geometric and electronic properties of a hybrid catalyst composed of [BMIM][TfO] and $(TiO_2)_n$ (n = 2–12) nanoclusters, and the HER catalytic activity was predicted by the density functional theory (DFT).[48] The calculation results show that the system ΔG of the hydrogen adsorption for the $[BMIM][TfO]/(TiO_2)_5$ is close to the ideal value (0 eV), suggesting a superior HER performance than that of the conventional Pt-based catalyst (Fig. 4).

Ionic liquids to improve electrolyte conduction

The electrolyte is also regarded as a key factor for determining the efficiency of an electrolysis system. The addition of an IL to aqueous electrolysis systems is promising to improve ion conductivity, reduce the activation energy, and modify the intrinsic structure of the electrode–electrolyte interfaces. The HER performance of various transition metal electrocatalysts (Ni, $FeCr_4$, $FeCr_8$, $FeMn_{12}$, Ni_{77}, and Mo) was tested using a 10 volume% aqueous solution of $[BMIM][BF_4]$ as the electrolyte.[49,50] These six electrodes showed high efficiencies in the range of 94.6%–99.2%, indicating that almost all the consumed charges were involved in hydrogen production. A particularly high electrochemical performance of 77.5 mA cm^{-2} at −1.7 V using a Pt quasi reference electrode (PtQRE) was achieved on the Mo electrodes, which can be explained by the enhanced proton donating properties of water on the preadsorbed imidazolium surface with reduced activation energy. Fiegenbaum et al. investigated the water electrolysis performance in an electrolyte of 0.1 M triethylammonium-propanesulfonic acid tetrafluoroborate ($[TEA-PS][BF_4]$).[51–53] The electrical

conductivity is 132.5 mS cm^{-1} for $[TEA-PS][BF_4]$, which is higher than those of $[BMIM][BF_4]$ (25.8 mS cm^{-1}), KOH (96.5 mS cm^{-1}), and KCl (52.3 mS cm^{-1}). In 0.1 M $[TEA-PS][BF_4]$, the HER current density of a PtNi/C catalyst increased significantly from 97 to 149 mA cm^{-2} at −2.0 V vs. PtQRE as the reaction temperature increasing from 25 to 80 °C, following a Volmer–Heyrovsky mechanism (Fig. 5). Subsequently, 0.1 M $[TEA-PS][BF_4]$ was applied for the HER study using vitreous carbon (VC), pyrolytic carbon (PC) and moulded graphite (MG) as the cathodic materials,[54] among which the VC and PC electrodes in 0.1 M $[TEA-PS][BF_4]$ presented higher performance compared to the Pt cathode, showing lower activation energy, higher cathodic exchange current, and lower charge transfer resistance. However, the use of MG for hydrogen production in this system is not recommended due to the deactivation of MG in 0.1 M $[TEA-PS][BF_4]$. Amaral et al. evaluated the effect of adding 1–2 vol% 1-ethyl-3-methylimidazolium acetate ([EMIM][Ac]), 1-ethyl-3-methylimidazolium ethyl sulfate ($[EMIM][EtSO_4]$) and 1-ethyl-3-methylimidazolium methanesulfonate ($[EMIM][MeSO_3]$) to an 8 M KOH electrolyte on the HER performance.[55] The best performance was obtained with the addition of 2 vol% $[EMIM][MeSO_3]$. The HER performance in IL-added KOH has a higher Tafel slope, lower overall impedance coefficient, and higher exchange current density than that in IL-free KOH, evidencing the importance of ILs as electrolyte additives. Amaral et al. studied 1-butyl-3-ethylimidazolium bromide [BEIM][Br] and 1,3-diethylimidazolium bromide [EEIM][Br] as the electrolyte additives with a content of 1–2 vol% in 8 M KOH for HER evaluation.[56] In general, the

Fig. 4 (a) ΔG for hydrogen evolution at equilibrium potential of the IL and $IL/(TiO_2)_n$ systems, (b) summary of calculated overpotentials for the IL and $IL/(TiO_2)_n$ systems, (c) HER activity volcano plot of exchange current [log (i_0)] plotted against ΔG of hydrogen adsorption in an acidic medium, and (d) schematic illustration of HER on the $IL/(TiO_2)_5$ system. Reproduced with permission.[48] Copyright 2021, American Chemical Society.

Fig. 5 (a) Effects of the potential on the current density with different electrolytes for water electrolysis: (a) $[BMIM][BF_4]$, (b) $[TEA-PS][BF_4]$, and (c) KOH, and (b) effects of temperature on the current density for 0.1 M $[TEA-PS][BF_4]$ at −2.0 V and −4.8 V. Current density (i) is expressed in mA cm^{-2}. Reproduced with permission.[50] Copyright 2013, Elsevier. (c) Tafel plots for the HER on Pt/C, PtNi/C and PtMo/C in 0.1 M $[TEA-PS][BF_4]$, and the (d) schematic representation of the Volmer–Heyrovsky mechanism for the HER. Reproduced with permission.[52] Copyright 2017, Elsevier.

bromine based ILs, with the exception of 2 vol% [EEIM][Br], which resulted in slight increases in Tafel slopes, could improve the electrolyte properties. Thimmappa *et al.* chose 10% diethylmethylammonium trifluoromethanesulfonate ([Dema-H][TfO]) aqueous solution as the electrolyte to study its effect on the HER and OER performance.[57] The study revealed that the IL–water system enabled two types of proton conduction, including H_3O^+ and $[Dema-H]^+$. The HER electrocatalysis was accelerated by the reduction of $[Dema-H]^+$ to $[Dema]$, and $[Dema]$ could be reprotonated at the anode by accepting protons from the OER.

In addition to adding ILs to aqueous electrolytes, ILs can also serve as polymer electrolyte additives for membrane electrode assemblies (MEAs). The protic IL [Dema-H][TfO] possessed good thermal stability, and high ionic conductivity at intermediate temperatures, and was used by Thimmappa *et al.* to fabricate a polymer electrolyte membrane based on a polytetrafluoroethylene (PTFE).[58] It was found that [Dema-H][TfO] almost completely filled the pores of the PTFE membrane. The low gas permeability was also confirmed by an H_2 crossover test, in which H_2 flowed to one side of the membrane (1 atm) and nitrogen flowed to the other side (50 cm^3 min^{-1}). As the temperature increased, the HER overpotential associated with the reduction of $[Dema-H]^+$ decreased by approximately 200 mV at 100 °C. The decrease in the HER overpotential with increasing temperature can be explained by the enhancement in kinetics and decrease in pK_a of $[Dema-H]^+$ with increasing temperature. A single cell water electrolyser with the [Dema-H][TfO] impregnated membrane was successfully operated at 100 °C and 50% RH. This shows good water uptake of protic IL from the vapor phase, which is promising for intermediate-temperature water electrolysis (Fig. 6).

Ionic liquid application in hydrogen storage

Due to their physicochemical properties, ILs have different roles to play in the field of hydrogen storage.[59] For example, light-weight and hydrogen-rich ILs can be used directly as hydrogen storage materials. Additionally, ILs can also be used as catalysts for dehydrogenation.
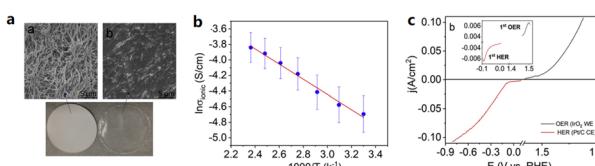
Fig. 6 (a) SEM surface morphology of (a) the unfilled PTFE membrane, (b) [Dema][TfO] impregnated PTFE membrane and below images of both membranes, (b) ionic conductivity of [Dema-H]$^+$[TfO]$^-$ filled in the PTFE membrane filter, and (c) OER and HER in IrO$_2$ and Pt/C MEA with humidified (100% RH) N$_2$ at 5 mV s^{-1} (inset figure for the lower potential region) at 20 °C. Reproduced with permission.[58] Copyright 2020, Elsevier.

ILs as hydrogen storage materials

The ILs with efficient hydrogen storage capacities were for the first time discovered by Doroodian *et al.*[60] Guanidinium-based borohydride ILs of $(N_3H_6)CBH_4$ and $(N_3H_8)CBH_4$ were obtained in tetrahydrofuran (THF) with guanidine chloride and sodium borohydride at 0 °C, as well as by mixing methyl-guanidine hydrochloride and sodium borohydride in the THF slurry at room temperature, respectively. The results indicated that $(N_3H_6)CBH_4$ had a good hydrogen storage capacity, *i.e.*, up to 10.7 wt% hydrogen, while for $(N_3H_8C)CBH_4$, 9.0 wt% hydrogen could be released under thermal and catalytic conditions. Their high capacity to release pure hydrogen rendered these ILs as promising hydrogen storage materials. Rekken *et al.*[61] developed a series of task-specific ILs: the *N*-substituted amine-borane ILs (N-ABILs), combining three different cations (imidazolium$^+$, pyrrolidinium$^+$, and pyrazolium$^+$) with three different anions (Cl$^-$, OTf$^-$, and Tf$_2$N$^-$), and their hydrogen storage capacity was investigated. It was found that the Cl-based IL had a higher capacity than OTf- and Tf$_2$N- based ILs. The optimized MeImEtABCl had a hydrogen storage capacity of 2.3 wt%. In addition, ILs can be mixed with other compounds to form liquid materials. For example, N-ABILs were mixed with amine-borane (AB) in different equivalents, resulting in improved hydrogen storage performance compared to pure N-ABILs. Using this strategy, EtImPrABTf$_2$N : AB with a ratio of 1 : 5 achieved a hydrogen storage capacity 4.9 wt%.

In contrast to the well-studied borohydride ILs, also known as tetrahydroborates (containing BH$_4$), octahydrotriborate ILs (containing B$_3$H$_8^-$) have also attracted a great deal of interest as intermediates in the thermal decomposition of borohydride ILs. For example, Chen *et al.*[62] prepared guanidine octahydrotriborate $((N_3H_6)C(B_3H_8))$ from NaB$_3$H$_8$ and guanidine chloride by ball milling or reaction in THF. Theoretically, $((N_3H_6)C(B_3H_8))$ possesses a hydrogen storage capacity of 13.8 wt% due to the feature of 6H in the cation and 8H in the anion. The corresponding dehydrogenation characteristics were investigated. The dehydrogenation occurred in multiple steps when the solution was treated at 100 °C. After 95 hours, approximately 6.5 equivalents or 12.9 wt% of hydrogen was released, with approximately 4 equivalents of hydrogen being released in the first hour.

In addition to the hydrogen storage properties of ammonia borane and borohydride ILs, five-membered B/N anionic chain complexes and liquid organic hydrogen carrier ILs also showed excellent hydrogen storage properties. For example, the synthesis and dehydrogenation of four kinds of five-membered B/N anionic chain ILs, [Bu$_4$N][BH$_3$(NH$_2$BH$_2$)$_2$H], [Et$_4$N][BH$_3$(NH$_2$BH$_2$)$_2$H], [C(N$_3$H$_6$)][BH$_3$(NH$_2$BH$_2$)$_2$H], and [C(N$_3$H$_5$CH$_3$)][BH$_3$(NH$_2$BH$_2$)$_2$H], were systematically investigated by Chen *et al.*[63] Fig. 7 shows the release of hydrogen from these four prepared IL aqueous solutions under the action of catalysts. Among the catalysts investigated, RuCl$_3$ showed excellent activity, catalyzing the release of hydrogen from all four ILs within 2 min (about 33–34 mL, 8 equivalents of hydrogen). The catalytic activities of NiCl$_2$ and Pt/C were similar, but
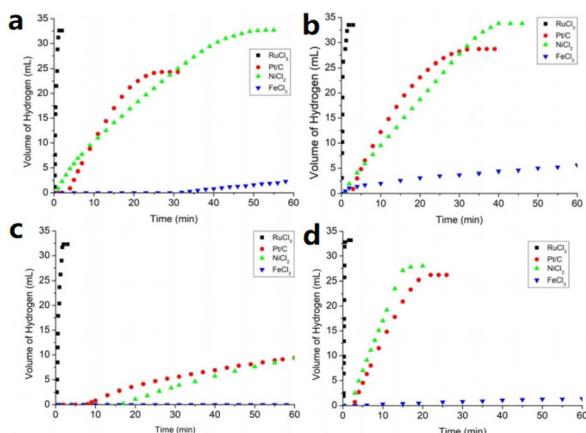
Fig. 7 Metal-catalyzed hydrolytic H_2 release from the aqueous solution of (a) $[Bu_4N][BH_3(NH_2BH_2)_2H]$, (b) $[Et_4N][BH_3(NH_2BH_2)_2H]$, (c) $[C(N_3H_6)][BH_3(NH_2BH_2)_2H]$, and (d) $[C(N_3H_5CH_3)][BH_3(NH_2BH_2)_2H]$ at room temperature.[63] Copyright 2021, Wiley-VCH.

Fig. 8 (a) Reaction paths involved in the preparation of imidazolium ionic liquids containing cyclohexane moieties. Reproduced with permission.[18] Copyright 2007, American Chemical Society. (b) New ionic liquids for hydrogen storage. Reproduced with permission.[64] Copyright 2020, Elsevier.

lower than that of $RuCl_3$, while no catalytic activity was observed for $FeCl_3$. This work provides insight into the ILs with the five-membered B/N anionic chain and further development of the chemistry of boron and nitrogen.

Hydrogenation of ILs was performed by Stracke et al.[18] and no hydrogenation of the imidazole ring was found, which means that in principle not any imidazole-based IL could be used as the liquid-organic hydrogen carrier (LOHC) system. Subsequently, Deyko et al.[64] developed ILs containing carbazole molecules as hydrogen-carrying sites using bis(trifluoromethylsulfonyl)imide imidazolium-based ILs (Fig. 8b), and compared the imidazole cation with carbazole. The results suggest that it was better to use the $-(CH_2)_3-$ linkers to connect N and Si atoms. N-(3-Trimethylsilylpropyl)carbazole was successfully hydrogenated with high selectivity and no byproduct with a low boiling point was formed. When the Pt/C was introduced as a hydrogenation and dehydrogenation catalyst, the theoretical total gravimetric hydrogen capacities of the synthesized ILs were 2.05 and 1.58 wt%, respectively.

Ionic liquids as dehydrogenation catalysts

ILs can serve as excellent catalysts for ammonia borane dehydrogenation.[65,66] For example, Sahler et al. tested the catalytic activities of various ILs towards the dehydrogenation of ethylene diamine bisborane (EDB).[67] It was found that the addition of certain ILs to EDB favors the dehydrogenation reaction. However, the adverse effects on the hydrogen yield (Fig. 9) also existed. The properties of imidazolium ILs are polarity-dependent, in which polar ILs are more favorable for the reaction than non-polar ones. A more in-depth study of 1-butyl-2,3-dimethylimidazolium chloride ([BMMIM][Cl]) showed that the [BMMIM]Cl/EDB mixture was capable of producing approximately 6.5 wt% hydrogen at 140 °C. The hydrogen content of morpholine borane is lower than that of ammonia borane, but the hydrogen production from morpholine borane is less expensive than from ammonia borane.
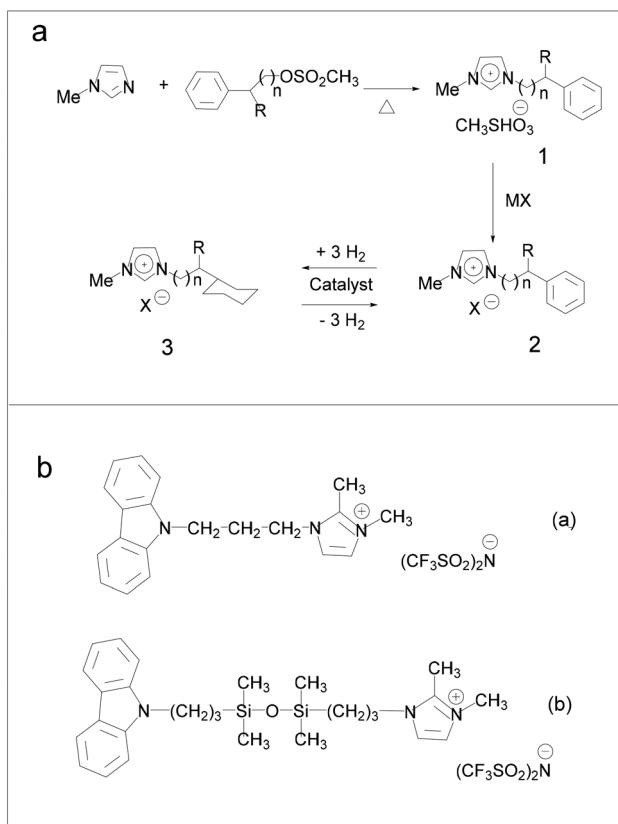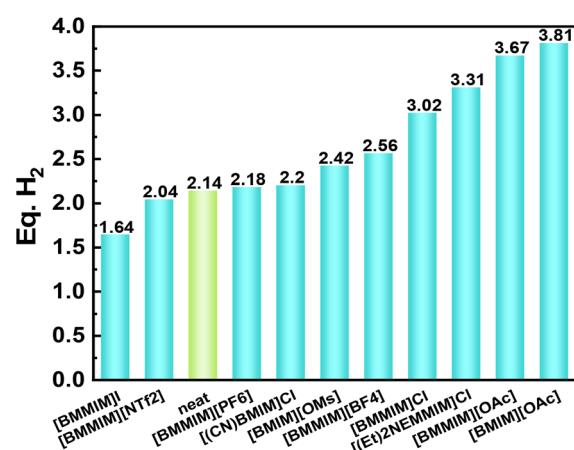
Fig. 9 Dehydrogenation yields of EDB supported by imidazolium-based ILs. Reproduced with permission.[67] Copyright 2013, Elsevier.

Mishra et al. investigated the thermal dehydrogenation of morpholine borane in the presence of ILs,[68] reporting the release of 1.46 equivalents of hydrogen at 60 °C and 1.75 equivalents of hydrogen at 80 °C. The amount of hydrogen released was
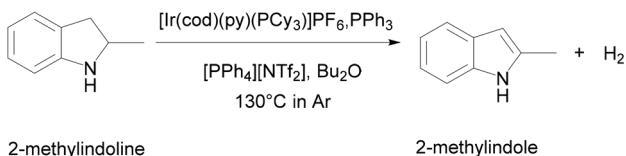
Fig. 10 Catalytic dehydrogenation of 2-methylindoline to 2-methyl-indole in the liquid−liquid biphasic catalyst system using Crabtree's cata-lyst. Reproduced with permission.[69] Copyright 2019, The Royal Society of Chemistry.

significantly higher than that released by the dehydrogenation of hydride solid without ILs, which was equivalent to 0.62 equivalents of hydrogen.

ILs are also excellent catalysts for LOHC. Søgaard et al. used a cationic iridium (Ir) complex immobilized in $[PPh_4][NTf_2]$ as a catalyst to study the dehydrogenation process (Fig. 10).[69] They combined a molten salt catalyst immobilisation strategy with a homogeneous catalyst to achieve efficient low-tempera-ture hydrogen storage/release of LOHC. Furthermore, the method allowed easy separation of catalyst and LOHC, enabling the release of large amounts of hydrogen and very small amounts of dissolved noble metal complexes.

Application of ionic liquids in hydrogen fuel cells

In recent decades, the development of new devices that can convert chemical energy to electricity has attracted extensive attention due to the gradually achieved global warming con-sensus.[70] In particular, the proton exchange membrane fuel cells (PEMFCs) that can directly convert hydrogen to electrical energy in an efficient way, is the star among all the candidates. Compared with internal combustion engines using fossil fuels, the PEMFCs not only decrease the energy demand but also eliminate carbon emission with the sole product of H_2O. However, the sluggish cathodic reaction (oxygen reduction reaction, ORR) kinetics and mass transfer are still the bottle-neck for the large-scale application of PEMFCs.[71] Generally, the ORR in fuel cells occurs at the triple-phase boundary (TPB) (electrocatalyst/electrolyte/oxygen), where electron transfer mainly occurs in the cathode catalyst layer, proton transfer in the ionomer, and gas transport through the gas diffusion layer. The limited TPB area is the main factor restricting the overall ORR performance due to the low utilization of cathode catalysts and poor proton conductivity.

Ionic liquids to enhance electrocatalyst activity

ILs, especially the protic ILs, have been deemed as effective additives for promoting the ORR performances[71,72] due to their high proton conductivity, great O_2 diffusion coefficiency, excellent electrochemical stability, and tunable hydrophobicity.[25,73] The concept of the "solid catalyst with IL

layer" (SCILL) was firstly proposed by U. Kernchen and col-leagues in 2007,[16] coating a thin IL film on a solid hetero-geneous electrocatalyst. Since then, many SCILL systems have been studied, exhibiting better activities in various reactions.[74,75] In 2010, Erlebacher et al.[76,77] for the first time implemented the hydrophobic SCILL concept in electrocataly-sis. The constructed nano-PtNi-[MTBD][beti] ([MTBD][beti]: 1-methyl-2,3,4,6,7,8-hexahydro-1H-pyrimidol[1,2-a]pyrimidi-nium bis(perfluoroethylsulfonyl)imide) composite catalysts exhibited 2–3 times higher intrinsic activity than their IL-free counterpart, and remarkably 10 times higher than Pt/C. The [MTBD]-based ILs were also reported to be effective at enhancing the ORR performances of Pt_3Ni nanoframes.[78] The capillary force of Pt_3Ni frames pulled the $[MTBD][NTf_2]$ into the pores, which retained the IL on the surface of the catalyst. The promoted ORR performances were attributed to the synergistic effects of material design and IL modifi-cations. Similarly, a GN-Pt-IL composite catalyst prepared by impregnating $[MTBD][NTf_2]$ into the pores of graphene sup-ported Pt nanoparticles showed improved ORR activity.[79] In addition to the benefits derived from the hydrophobicity and great proton diffusion, the unique less methanol-philic feature of $[MTBD][NTf_2]$ ensured a high methanol tolerance of the electrocatalysts. Besides $[MTBD]^+$-based ILs, a variety of other ILs are also reported to greatly boost the ORR. For example, Luo et al.[80] prepared a well-connected and stable proton path for high-temperature PEMFCs by adding 1-hexyl-3-methylimidazolium trifluoromethansulfonate $([C_6MIM][CF_3SO_3])$ to the Pt electrocatalyst. Benefiting from the efficient proton delivery and IL-protector layer, the modified Pt catalyst exhibited a maximum power density (P_{max}) of 512 mW cm^{-2} and 10% performance loss after 100 k cycles of stability test, which was superior to the durability performance of commercial Pt/C. Doblinger et al.[81] com-pared the promotion effects of a broad range of IL cations and anion combinations (imidazolium, ammonium, phos-phonium, pyrrolidinium anions and $[BF_4]^-$, $[PF_6]^-$, $[NTf_2]^-$, $[FAP]^-$ cations) at different humidity levels. The cations were found to affect the ORR current density within a wide humidity range; the anions were proven to influence the performance at a humidity level higher than 65% RH. This work pointed out that the optimal choice of the IL promoter needed to consider the humidity in the PEMFC cell. The protic ILs were also reported to be capable of replacing ionomers in the electrode for the ORR. Li et al.[82] investigated the ORR performances of Pt/C under the conditions with sulfonated PIL ionomers only and a mixture of PIL ionomer/Nafion. The results suggested that the Pt/C with only the sulfonated PILs out-performed by 2 times due to the suppressed Pt oxidation, while the advantages on kinetics severely dropped at lower humidity levels. By appropriately combining PILs with Nafion, the high ORR activity was maintained across a wide humidity range. Yan et al.[73] completely replaced Nafion with poly(DMVBA$_n$-TfO-co-St$_m$) in the Pt/C electroca-talysts and achieved a 3.06 times higher performance than

their Nafion-Pt/C counterpart. Besides the general explanations of the improved ORR activity, the PIL ionomers were believed to also suppress the nonreactive oxygenate adsorption on the Pt active sites.

Many efforts in the literature are devoted to disclosing the mechanisms underlying the positive effects of ILs. In the case of enhanced proton conductivity, recent work by Wang *et al.*[83] proved proton shuffling promotional effects of ILs on the ORR needed fine tuning. The authors screened a series of ILs as additives to Pt/C for the ORR and found a volcano correlation between ORR activities and pK_a values. [MTBD][NTf₂] was proven to be an optimal promoter with a pK_a of approximately 15, which was close to the pK_a of the product of the ORR rate-limiting step: H_2O ($pK_a = 15.7$). The "perfect match" of the pK_a value and facilitated ORR performance were attributed to the hydrogen-bonding structure and the tunneling transfer of the proton. The larger product of Boltzmann probability and the proton vibration wavefunction overlap the integral of [MTBD] $N-H^+ \cdots OH_{Pt}$, $P_\mu S_{\mu\nu}^2$. With matched pK_a, the largest $P_\mu S_{\mu\nu}^2$ indicates a much higher hydrogen tunneling rate/probability for the ORR rate-determining step. The correlation between IL acidities and promotion effects on ORR activity was also investigated by Wippermann *et al.*[84] In addition, Zhang *et al.*[85] found that the Pt/C ORR performance had a strong dependence on the cationic side-chain length of imidazolyl ILs. If the alkyl chains were too short (*e.g.*, 1-ethyl-3-methylimidazolium bis(trifluoromethanesulfonyl)imide ([EMIM][NTf₂])), the IL could not sufficiently enhance ORR activity because of their limited hydrophobicity as well as the low capability of suppressing the formation of nonreactive oxygenated species on Pt.

By contrast, the IL with too long alkyl chains (*e.g.*, 1-hexyl-3-methylimidazolium bis(trifluoromethanesulfonyl)imide ([C₆MIM][NTf₂]) and 1-decyl-3-methylimidazolium bis(trifluoromethanesulfonyl)imide ([C₁₀MIM][NTf₂])) would lead to a significant loss of the electrochemical active surface area (ECSA). The optimal chain length was needed to achieve a balance between effective inhibition of the formation of oxygenated species on the Pt surface and less passivation of active sites. Avid *et al.*[86] further emphasized the roles of IL in the porous structure of the Pt/C in improving the ORR performance. The alkyl imidazolium ILs with different alkyl chain lengths were loaded into the Pt/C and the impacts of the IL chemical structure on the ORR performance were investigated. As shown in Fig. 11a and b, the ILs that could penetrate into the pores of carbon black would significantly enhance the proton and O_2 transfer inside the pores. Additionally, the impacts of ILs on the ORR activity were conformational structure-dependent. Fig. 11c and d show that the combination of butyl and methyl functional groups promoted the ORR activity of Pt/C the most. By contrast, the butyl/methyl and butyl/bimethyl functioned imidazolium-based ILs were less beneficial or even detrimental. The authors highlighted the trade-off between proton conductivity and O_2 transfer resistance, and pointed out the important roles of electrochemical ECSA change, pore-filling degree, hydrophobicity, and attraction/repulsion with Nafion in the rational design of SCILL towards the ORR.
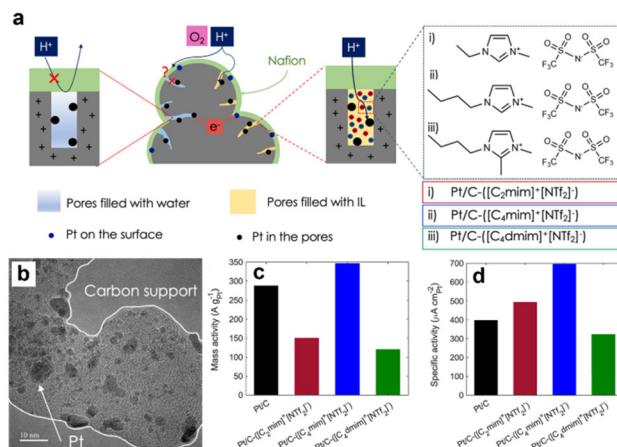
Fig. 11 (a) The scheme of the ILs filled in the pores of carbon black supports. (b) The TEM images of Pt/C-IL catalysts. The gravimetric performance (c) and geometric performance (d) comparisons of catalysts modified with different ILs. Reproduced with permission from ref. 86. Copyright 2022, Springer Nature.

Although the IL promotional effects are conventionally ascribed to the enhanced O_2 transfer, quantitative investigations on the transfer resistances are relatively rare in the literature. Recently, Huang *et al.*[87] have used the 1-methyl-2,3,4,6,7,8-hexa-hydro-1*H*-pyrimido[1,2-*a*]pyrimidinium 1,1,2,2,3,3,4,4,4-nona-fluorobutane-1-sulfonate ([MTBD][C₄F₉SO₃]) IL and boosted the ORR performance of PtCo/C by 48%. By conducting the limiting current measurements at different O_2 partial pressures, the O_2 transfer resistances were quantitatively determined. The results suggested that the IL resulted in an approximately 15% drop in oxygen diffusion resistances compared to its counterpart in the same electrode structure. In addition, the PtCo/C + IL showed a more durable O_2 diffusion resistance during the 30 k cycles of stability tests, which was significantly better than the pristine PtCo/C. Another nontrivial mechanism of the IL-enhanced ORR is that the ILs alleviated the specific adsorption of the sulfonate functional group of Nafion on the Pt surface, which was detrimental to the ORR activity[88,89] according to the ATR-SEIRAS method used to quantitatively investigated the specific adsorption of sulfonate anions. In the absence of ILs, the $-SO_3^-$ specific adsorption was visible at 1125 cm^{-1}. By contrast, after introducing [MTBD][beti] ILs, the vibrational absorption of $-SO_3^-$ in the IR spectra diminished within the investigated polarization potentials.

Ionic liquids to improve electrocatalyst stability

Moreover, the electrochemical stability of Pt electrocatalysts could also be improved by introducing ILs *via* preventing Pt nanoparticles agglomeration, surface oxidation, and carbon corrosion mechanisms. In the pioneering works of SCILLs,[90–93] the ILs including [MTBD]⁺, [BMIM]⁺ cations, *etc.*, were proven to be beneficial for the durability of ORR electrocatalysts. More recently, Li *et al.*[94] have synthesized an ultra-thin PtFeNi nanowire loaded with the 1-(3-aminopropyl)-3-

methylimidazolium bromide IL forming a conjugated structure (Fig. 12a). As shown in Fig. 12c, the PtFeNi nanowire/IL exhibited a high ORR activity at 2.83 A mg_{Pt}^{-1}, which improved by 172% compared with the pristine PtFeNi. After 30 k cycles, the morphology and performance were largely maintained, and the durability was remarkably higher than the control group sample without IL modification (Fig. 12b and c). Li et al.[95] reported a process to load the IL within the 3D catalyst layer forming an optimal conformational structure of the electrode. As shown in Fig. 12d, the porous catalyst layer was charged positively and dipped into the IL solution. The IL anions were uniformly distributed in the porous catalyst layer driven by the electrostatic force. The subsequent ion-exchange with IL cations resulted in a well-constructed protic IL film across the electrode hierarchical structure. Following this procedure, the authors prepared the Pt/C electrocatalyst with a ~2 nm [MTBD][beti] IL coating. The Pt/C-[MTBD][beti] electrocatalysts showed an improvement of ORR activity by a factor of ~2 compared to Pt/C (Fig. 12e). The durability was also improved after loading the ILs. As presented in Fig. 12f, the Pt/C + [MTBD][beti] exhibited remarkable advantages in durability with less than 30% ORR performance loss compared with Pt/C after 10 k cycles at the upper potential limit. The improved durability was attributed to the capability of maintaining the ECSA and much less Pt loss (Fig. 12g and h). The

IL layer was believed to reduce the H*, destabilize OOH* and interrupt the hydrogen-bonding water network. Avid et al.[86] further suggested that both the chemical structure of ILs and the conformational structure of the whole electrode were crucial to the ORR durability improvements. Since the performance of Pt degraded faster in contact with water than ionomer,[96] the IL molecules with an appropriate alkyl chain length and interaction with Pt benefited durability the most. Because most of the Pt nanoparticles were within the pores of activated carbon, the capability of ILs to access the pores would improve the durability, which will also reduce the possibility of ILs to wash off during ORR tests. It is also important to note that ILs are not always beneficial for durability. For example, George et al.[97] conducted an in situ ICP-MS investigation on the PtNiMo/C electrocatalyst degradation mechanism with and without IL modification. It was found that [MTBD][Beti] IL selectively increased the leaching of Mo elements in the PtNiMo/C electrocatalyst, though the mass activity was promoted by 70%.

In summary, ILs have been proven effective in promoting the performances as well as enhancing the durability of electrocatalytic ORR via regulating the hydrogen bonding, hydrophobicity, proton/O_2 transfer resistance, oxygenated species suppression, etc. Comparing the prosperous new catalyst developments, ILs are still limited to relatively few candidates. Although the general mechanisms underpinning the IL promotional effects have been proposed, quantitative investigations to prove a solid correlation between IL chemical–physical properties and specifically enhanced ORR kinetics are still lacking. The accurate description of the conformational structures of the IL-modified catalysts layer is still ambiguous. As a prosperous research topic of PEMFCs, new ILs with a clear understanding of the correlation between their structure and promotional effects are expected to further advance both the catalytic activities and durability of ORR electrocatalysis.

Summary and perspective

Hydrogen energy is deemed the most promising carbon-free secondary energy source and will fundamentally reshape both the industry and our modern way of life. Before a future powered by hydrogen energy becomes a reality, there are still important scientific challenges to be addressed within the scope of its production, transportation, and utilization. As summarized in this review, ILs, a class of green, highly designable organic compounds, have been proven to be capable of acting as a new cornerstone in all these aspects mentioned above, including but not limited to the roles of catalysts, catalyst supports and promoters, catalyst preparation regulators and hydrogen carriers. We should also be aware of the potential drawbacks of certain ILs, such as susceptibility to moisture in the air, potential environmental toxicity, and high cost, as well as the difficulty of recycling them in hydrogen energy applications, such as for catalyst synthesis and interface microenvironment enhancement. To further advance this emerging

Fig. 12 The TEM bright-field images of PtFeNi nanowires + ILs (a) before and (b) after 30 k cycles of durability tests. The ORR activities of PtFeNi nanowires + ILs and control group samples (c) before and after the stability tests. Reproduced with permission from ref. 94. Copyright 2019, Elsevier. (d) The scheme of sequential procedure loading [MTBD][beti] onto Pt/C electrocatalysts and the corresponding TEM image of Pt/C + IL. The (e) ORR activities of fresh Pt/C + [MTBD][beti] and Pt/C. The (f) ORR activities loss, (g) ECSA retaining ratios and (h) Pt concentrations in the electrolyte of Pt/C + [MTBD][beti] and Pt/C after the accelerated durability tests. Reproduced with permission from ref. 95. Copyright 2019, Copyright 2019, American Chemical Society.

research area, the essential scientific questions for future in-depth investigations are proposed subsequently.

In the case of ILs acting as catalyst supports and promoters, the understanding of the spatial and electronic relationship between the catalysts and the ILs is still limited. For catalysts with porous structures, the configurations of the ILs filled inside the pores and the effects of the confined structure on the functions of the ILs are less investigated. On the other hand, the PILs can also provide meso/microporous structures for catalysts. The confinement effects of PILs, including electronic, chemical, and steric effects, on the catalytic performances are still ambiguous. Another key issue is the stability of the IL catalyst composite structure. Considering that the IL-promoted catalytic reactions usually take place in a liquid environment with vigorous stirring, the leaching of ILs from the IL catalyst composites needs careful consideration. Finally, with the involvement of ILs in a catalytic reaction makes the mechanisms quite complex. *In situ* spectrokinetic characterization with high spatial/time resolutions and theoretical calculations on multi-scales are proposed to unravel the accurate and comprehensive reaction networks.

ILs acting as catalyst preparation regulators can enable the production of catalysts with different morphologies, sizes, and structures compared to conventional surfactants. However, the origin of these unique structures and the interaction of ILs with catalysts during the preparation process is less well understood. Time-resolved investigations on the morphology/crystalline structure evolution of catalysts during the IL-assisted preparation are highly recommended. Spectroscopic and theoretical investigations on the interaction between ILs and crystallites are required to disclose the mechanisms underlying the regulation effects.

Compared with conventional hydrogen storage organics, ILs show some unique advantages, including extremely low vapor pressure, high H_2 storage density, self-catalytic effects, *etc*. For their practical application, the weight, cost penalty, and potential biological and environmental toxicity of certain ILs added to the hydrogen storage system would need to be addressed. The reversibility of ILs during H_2 storage/release requires further evaluation.

Conflicts of interest

There are no conflicts to declare.

Acknowledgements

References

1 X. Yang, C. P. Nielsen, S. J. Song and M. B. McElroy, *Nat. Energy*, 2022, **7**, 955–965.

2 X. Hou, L. Yang, K. Hou, H. Shi, L. Feng, G. Suo, X. Ye, L. Zhang and Y. Yang, *Green Energy Environ.*, 2021, **6**, 124–137.

3 G. Yang, S. Guan, S. Mehdi, Y. Fan, B. Liu and B. Li, *Green Energy Environ.*, 2021, **6**, 236–243.

4 R. Kun-udom, S. Jantarang, Z. Du, B. Kitiyanan, T. Rirksomboon and V. Meeyoo, *Green Chem. Eng.*, 2022, **3**, 44–54.

5 J. Rafiee, X. Mi, H. Gullapalli, A. V. Thomas, F. Yavari, Y. Shi, P. M. Ajayan and N. A. Koratkar, *Nat. Mater.*, 2012, **11**, 217–222.

6 R. Hanna and D. G. Victor, *Nat. Energy*, 2021, **6**, 568–571.

7 B. Pivovar, N. Rustagi and S. Satyapal, *Electrochem. Soc. Interface*, 2018, **27**, 47–52.

8 S. Zhang, X. Zhang, Y. Rui, R. Wang and X. Li, *Green Energy Environ.*, 2021, **6**, 458–478.

9 M. F. Lagadec and A. Grimaud, *Nat. Mater.*, 2020, **19**, 1140–1150.

10 C. Tarhan and M. A. Çil, *J. Energy Storage*, 2021, **40**, 102676.

11 R. Singh, M. Singh and S. Gautam, *Mater. Today: Proc.*, 2021, **46**, 5420–5427.

12 S. Chatterjee, R. K. Parsapur and K.-W. Huang, *ACS Energy Lett.*, 2021, **6**, 4390–4394.

13 S. Favero, I. E. L. Stephens and M. M. Titirici, *Adv. Energy Sustainability Res.*, 2021, **2**, 2000062.

14 C. Verma, E. E. Ebenso and M. A. Quraishi, *J. Mol. Liq.*, 2019, **276**, 826–849.

15 K. Chen, B. Xu, L. Y. Shen, D. H. Shen, M. J. Li and L. H. Guo, *RSC Adv.*, 2022, **12**, 19452–19469.

16 U. Kernchen, B. Etzold, W. Korth and A. Jess, *Chem. Eng. Technol.*, 2007, **30**, 985–994.

17 X. Tan, X. Sun and B. Han, *Natl. Sci. Rev.*, 2022, **9**, nwab022.

18 M. P. Stracke, G. Ebeling, R. Cataluña and J. Dupont, *Energy Fuels*, 2007, **21**, 1695–1698.

19 M. E. Bluhm, M. G. Bradley, R. Butterick, U. Kusari and L. G. Sneddon, *J. Am. Chem. Soc.*, 2006, **128**, 7748–7749.

20 V. Thamke, P. Singh, S. Pal, M. Chaudhary, K. Kumari, I. Bahadur and R. S. Varma, *J. Environ. Chem. Eng.*, 2022, **10**, 107303.

21 R. L. Vekariya, *J. Mol. Liq.*, 2017, **227**, 44–60.

22 G. Kaur, H. Kumar and M. Singla, *J. Mol. Liq.*, 2022, **351**, 118556.

23 F. Li, F. Mocci, X. Zhang, X. Ji and A. Laaksonen, *Chin. J. Chem. Eng.*, 2021, **31**, 75–93.

24 O. S. Hammond and A. V. Mudring, *Chem. Commun.*, 2022, **58**, 3865–3892.

25 H. A. Elwan, M. Mamlouk and K. Scott, *J. Power Sources*, 2021, **484**, 229197.

26 A. Nasri, B. Jaleh, E. Shabanlou, M. Nasrollahzadeh, H. A. Khonakdar and B. Kruppke, *J. Mol. Liq.*, 2022, **365**, 120142.

27 S. Sahler and M. H. G. Prechtl, in *Hydrogen Storage*, ed. L. Jianjun, IntechOpen, Rijeka, 2012, ch. 6, pp. 147–164, DOI: **10.5772/50154**.

28 A. Alashkar, A. Al-Othman, M. Tawalbeh and M. Qasim, *Membranes*, 2022, **12**, 178.

29 Y. Tian, Y. R. Liu, H. Wang, L. Liu and W. P. Hu, *ACS Sustainable Chem. Eng.*, 2022, **10**, 4345–4358.

30 B. Yang, W. L. Ding, H. H. Zhang and S. J. Zhang, *Energy Environ. Sci.*, 2021, **14**, 672–687.

31 V. W. H. Lau, A. F. Masters, A. M. Bond and T. Maschmeyer, *Chem. – Eur. J.*, 2012, **18**, 8230–8239.

32 J. Ye, Z. Yu, W. Chen, Q. Chen, S. Xu and R. Liu, *Carbon*, 2016, **107**, 711–722.

33 X. Zhang, H. Li, H. Yang, F. Xie, Z. H. Yuan, L. Zajickova and W. J. Li, *ChemElectroChem*, 2020, **7**, 3347–3352.

34 Y. X. Liu, Z. M. Tian, Q. C. Xu, Y. X. Yang, Y. T. Zheng, H. G. Pan, J. Chen, Z. Wang and W. J. Zheng, *ACS Appl. Mater. Interfaces*, 2022, **14**, 8963–8973.

35 Y. Zhang, C. Li, Z. Chen, Y. Ni, F. Kong, A. Kong and Y. Shan, *Catal. Lett.*, 2017, **147**, 253–260.

36 C. Y. Zhang, B. W. Xin, Z. C. Xi, B. H. Zhang, Z. Y. Li, H. Zhang, Z. H. Li and J. C. Hao, *ACS Sustainable Chem. Eng.*, 2018, **6**, 1468–1477.

37 D. M. Tang, T. H. Li and C. M. Li, *Int. J. Hydrogen Energy*, 2019, **44**, 1720–1726.

38 H. Ying, C. Zhang, T. Chen, X. Zhao, Z. Li and J. Hao, *Nanotechnology*, 2020, **31**, 505402.

39 J. H. Tong, W. M. Ma, L. L. Bo, T. Li, W. Y. Li, Y. L. Li and Q. Zhang, *J. Power Sources*, 2019, **441**, 227166.

40 D. L. Zhang, H. Y. Mou, L. Chen, D. B. Wang and C. X. Song, *Appl. Surf. Sci.*, 2020, **510**, 145483.

41 J. Sun, N. K. Guo, Z. Y. Shao, K. K. Huang, Y. W. Li, F. He and Q. Wang, *Adv. Energy Mater.*, 2018, **8**, 1800980.

42 H. Mao, X. Guo, Q. Fan, Y. Fu, H. Yang, D. Liu, S. Wu, Q. Wu and X.-M. Song, *Chem. Eng. J.*, 2021, **404**, 126253.

43 M. R. Gao, S. H. Yu, J. Y. Yuan, W. Y. Zhang and M. Antonietti, *Angew. Chem., Int. Ed.*, 2016, **55**, 12812–12816.

44 Y. X. Ding, A. Klyushin, X. Huang, T. Jones, D. Teschner, F. Girgsdies, T. Rodenas, R. Schlogl and S. Heumann, *Angew. Chem., Int. Ed.*, 2018, **57**, 3514–3518.

45 L. Gidi, R. Arce, J. Ibarra, M. Isaacs, M. J. Aguirre and G. Ramirez, *Electrochim. Acta*, 2021, **372**, 137859.

46 S. Ji, T. Li, Z.-D. Gao, Y.-Y. Song and J.-J. Xu, *Chem. Commun.*, 2018, **54**, 8765–8768.

47 T. N. P. Truong, H. Randriamahazaka and J. Ghilane, *ACS Catal.*, 2018, **8**, 869–875.

48 D. K. Pandey, H. L. Kagdada, A. Materny and D. K. Singh, *J. Phys. Chem. A*, 2021, **125**, 2653–2665.

49 G. Loget, J. C. Padilha, E. A. Martini, M. O. de Souza and R. F. de Souza, *Int. J. Hydrogen Energy*, 2009, **34**, 84–90.

50 R. F. de Souza, G. Loget, J. C. Padilha, E. M. A. Martini and M. O. de Souza, *Electrochem. Commun.*, 2008, **10**, 1673–1675.

51 F. Fiegenbaum, E. M. Martini, M. O. de Souza, M. R. Becker and R. F. de Souza, *J. Power Sources*, 2013, **243**, 822–825.

52 D. W. Lima, F. Fiegenbaum, F. Trombetta, M. O. de Souza and E. M. A. Martini, *Int. J. Hydrogen Energy*, 2017, **42**, 5676–5683.

53 F. Fiegenbaum, M. O. de Souza, M. R. Becker, E. M. A. Martini and R. F. de Souza, *J. Power Sources*, 2015, **280**, 12–17.

54 D. W. Lima, F. Fiegenbaum, F. Trombetta, M. O. de Souza and E. M. A. Martini, *Int. J. Hydrogen Energy*, 2018, **43**, 1239–1250.

55 L. Amaral, D. S. P. Cardoso, B. Šljukić, D. M. F. Santos and C. A. C. Sequeira, *Mater. Res. Bull.*, 2019, **112**, 407–412.

56 L. Amaral, J. Minkiewicz, B. Sljukic, D. M. F. Santos, C. A. C. Sequeira, M. Vranes and S. Gadžurić, *ECS Trans.*, 2018, **86**, 711–717.

57 R. Thimmappa, D. Walsh, K. Scott and M. Mamlouk, *J. Power Sources*, 2020, **449**, 227602.

58 R. Thimmappa, K. Scott and M. Mamlouk, *Int. J. Hydrogen Energy*, 2020, **45**, 28303–28312.

59 M. H. G. Prechtl and S. Sahler, *Curr. Org. Chem.*, 2013, **17**, 220–228.

60 A. Doroodian, J. E. Dengler, A. Genest, N. Rösch and B. Rieger, *Angew. Chem., Int. Ed.*, 2010, **49**, 1871–1873.

61 B. D. Rekken, A. E. Carre-Burritt, B. L. Scott and B. L. Davis, *J. Mater. Chem. A*, 2014, **2**, 16507–16515.

62 W. D. Chen, Z. G. Huang, G. T. Wu, T. He, Z. Li, J. E. Chen, Z. P. Guo, H. K. Liu and P. Chen, *J. Mater. Chem. A*, 2015, **3**, 11411–11416.

63 X. M. Chen, X. Jiang, Y. Jing and X. N. Chen, *Chem. – Asian J.*, 2021, **16**, 2475–2480.

64 G. S. Deyko, L. M. Glukhov and L. M. Kustov, *Int. J. Hydrogen Energy*, 2020, **45**, 33807–33817.

65 S. Sahler, S. Sturm, M. T. Kessler and M. H. G. Prechtl, *Chem. – Eur. J.*, 2014, **20**, 8934–8941.

66 D. W. Himmelberger, L. R. Alden, M. E. Bluhm and L. G. Sneddon, *Inorg. Chem.*, 2009, **48**, 9883–9889.

67 S. Sahler, H. Konnerth, N. Knoblauch and M. H. G. Prechtl, *Int. J. Hydrogen Energy*, 2013, **38**, 3283–3290.

68 D. K. Mishra, R. Hussain, G. Pugazhenthi and T. Banerjee, *ACS Sustainable Chem. Eng.*, 2022, **10**, 6157–6164.

69 A. Søgaard, M. Scheuermeyer, A. Bösmann, P. Wasserscheid and A. Riisager, *Chem. Commun.*, 2019, **55**, 2046–2049.

70 J. Y. Cui, Q. J. Chen, X. J. Li and S. J. Zhang, *Green Chem.*, 2021, **23**, 6898–6925.

71 S. Hu, J. Wang, J. Zhang, J. Lim, Y. Gao and S. Zhang, *Appl. Catal., B*, 2021, **282**, 119593.

72 D. E. Smith and D. A. Walsh, *Adv. Energy Mater.*, 2019, **9**, 1900744.

73 X. Yan, F. Zhang, H. Zhang, H. Tang, M. Pan and P. Fang, *ACS Appl. Mater. Interfaces*, 2019, **11**, 6111–6117.

74 H. P. Steinruck, J. Libuda, P. Wasserscheid, T. Cremer, C. Kolbeck, M. Laurin, F. Maier, M. Sobota, P. S. Schulz and M. Stark, *Adv. Mater.*, 2011, **23**, 2571–2587.

75 J. Arras, M. Steffan, Y. Shayeghi, D. Ruppert and P. Claus, *Green Chem.*, 2009, **11**, 716–723.

76 J. Snyder, T. Fujita, M. W. Chen and J. Erlebacher, *Nat. Mater.*, 2010, **9**, 904–907.

77 J. Snyder, K. Livi and J. Erlebacher, *Adv. Funct. Mater.*, 2013, **23**, 5494–5501.

78 C. Chen, Y. Kang, Z. Huo, Z. Zhu, W. Huang, H. L. Xin, J. D. Snyder, D. Li, J. A. Herron, M. Mavrikakis, M. Chi, K. L. More, Y. Li, N. M. Markovic, G. A. Somorjai, P. Yang and V. R. Stamenkovic, *Science*, 2014, **343**, 1339–1343.

79 Y. Tan, C. Xu, G. Chen, N. Zheng and Q. Xie, *Energy Environ. Sci.*, 2012, **5**, 6923–6927.

80 F. Luo, Q. Zhang, Z. Yang, L. Guo, X. Yu, K. Qu, Y. Ling, J. Yang and W. Cai, *ChemCatChem*, 2018, **10**, 5314–5322.

81 S. Doblinger, J. Lee and D. S. Silvester, *J. Phys. Chem. C*, 2019, **123**, 10727–10737.

82 Y. Li, T. Van Cleve, R. Sun, R. Gawas, G. Wang, M. Tang, Y. A. Elabd, J. Snyder and K. C. Neyerlin, *ACS Energy Lett.*, 2020, **5**, 1726–1731.

83 T. Wang, Y. Zhang, B. Huang, B. Cai, R. R. Rao, L. Giordano, S.-G. Sun and Y. Shao-Horn, *Nat. Catal.*, 2021, **4**, 753–762.

84 K. Wippermann, Y. Suo and C. Korte, *J. Phys. Chem. C*, 2021, **125**, 4423–4435.

85 G. R. Zhang, T. Wolker, D. J. S. Sandbeck, M. Munoz, K. J. J. Mayrhofer, S. Cherevko and B. J. M. Etzold, *ACS Catal.*, 2018, **8**, 8244–8254.

86 A. Avid, J. L. Ochoa, Y. Huang, Y. Liu, P. Atanassov and I. V. Zenyuk, *Nat. Commun.*, 2022, **13**, 6349.

87 K. Huang, H. Lin, L. Zhou, L. Wang and H. Jia, *J. Electrochem. Soc.*, 2022, **169**, 044516.

88 S. Holdcroft, *Chem. Mater.*, 2014, **26**, 381–393.

89 J. Tymoczko, F. Calle-Vallejo, V. Colic, M. T. M. Koper, W. Schuhmann and A. S. Bandarenka, *ACS Catal.*, 2014, **4**, 3772–3778.

90 G. R. Zhang, M. Munoz and B. J. M. Etzold, *ACS Appl. Mater. Interfaces*, 2015, **7**, 3562–3570.

91 G. R. Zhang, M. Munoz and B. J. M. Etzold, *Angew. Chem., Int. Ed.*, 2016, **55**, 2257–2261.

92 K. Huang, T. Q. M. Song, O. Morales-Collazo, H. F. Jia and J. F. Brennecke, *J. Electrochem. Soc.*, 2017, **164**, F1448–F1459.

93 Q. C. Tran, V.-D. Dao, H. Y. Kim, K.-D. Jung and H.-S. Choi, *Appl. Catal., B*, 2017, **204**, 365–373.

94 C. J. Li, B. L. Huang, M. C. Luo, Y. N. Qin, Y. J. Sun, Y. J. Li, Y. Yang, D. Wu, M. G. Li and S. J. Guo, *Appl. Catal., B*, 2019, **256**, 117828.

95 Y. W. Li, J. Hart, L. Profit, S. Intikhab, S. Chatterjee, M. Taheri and J. Snyder, *ACS Catal.*, 2019, **9**, 9311–9316.

96 A. Perego, A. Avid, D. N. Mamania, Y. Chen, P. Atanassov, H. Yildirim, M. Odgaard and I. V. Zenyuk, *Appl. Catal., B*, 2022, **301**, 120810.

97 M. George, G. R. Zhang, N. Schmitt, K. Brunnengräber, D. J. S. Sandbeck, K. J. J. Mayrhofer, S. Cherevko and B. J. M. Etzold, *ACS Catal.*, 2019, **9**, 8682–8692.